Detection of rice sheath blight for in-season disease management using multispectral remote sensing

Zhihao Qin [a,b], Minghua Zhang [a,*]

[a] *Department of Land Air and Water Resources, University of California, Davis, CA 95616, USA*
[b] *Institute of Agricultural Resources and Regional Planning, Chinese Academy of Agricultural Sciences, Beijing 100081, China*

Abstract

Timely diagnosis of crop diseases in fields is critical for precision on-farm disease management. Remote sensing technology can be used as an effective and inexpensive method to identify diseased plants in a field scale. However, due to the diversity of crops and their associated diseases, application of the technology to agriculture is still in research stage, which needs to be elaborately investigated for algorithm development and standard image processing procedures. In this paper, we examined the applicability of broadband high spatial-resolution ADAR (Airborne Data Acquisition and Registration) remote sensing data to detect rice sheath blight and developed an approach to further explore the applicability. Based on the field symptom measurements, a comprehensive field disease index (DI) was constructed to measure infection severity of the disease and to relate to image sampled infections. In addition to direct band digital number (DN) values, band ratio indices and standard difference indices were used to examine possible correlations between field and image data. The results indicated that the broadband remote sensing imagery has the capability to detect the disease. Some image indices such as RI_{14}, SDI_{14} and SDI_{24} worked better than others. A correlation coefficient above 0.62 indicated that these indices would be valuable to use for identification of the rice disease. In the validation analysis, we obtained a small root mean square error (RMS = 9.1), confirming the applicability of the developed method. Although the results were encouraging, it was difficult to discriminate healthy plants from light infection ones when DI < 20 because of their spectral similarities. Hence, it was clear that identification accuracy increases when infection reaches medium-to-severe levels (DI > 35). This phenomenon illustrated that remote sensing images with higher spectral resolution (more bands and narrower bandwidth) were required in order to further examine the capability of separating the light diseased plants from healthy plants.
© 2005 Elsevier B.V. All rights reserved.

Keywords: Rice disease; Remote sensing; Sheath blight; Agriculture; Crop; Diagnosis

1. Introduction

Rice is an important crop worldwide and over half of the world population relies on it for food. Sustainable farming of rice depends on many factors including

* Corresponding author. Tel.: +1 530 752 4953;
fax: +1 530 752 5262.
 E-mail address: mhzhang@ucdavis.edu (M. Zhang).

effective and timely pest management to protect the crop. Remote sensing has the potential to be used as an effective and inexpensive technique to identify diseased plants in a field scale, mainly because infected plants have different spectral response compared to healthy plants (Zhang et al., 2002).

Studies on remote sensing applications to crop diseases are very few (Zhang et al., 2003) though the potential for application of remote sensing techniques to epidemiological problems has long been argued (Cline, 1970). Current epidemiological application of remote sensing is essentially a mapping exercise to demonstrate the relevant ecological variables and processes that can be observed remotely (Hay, 1997). Quantitative analysis of remote sensing data for diseased crop identification has not been extensively studied, in spite of being a potential application of remote sensing to crop disease control.

As to rice remote sensing, most studies were focused on field area mapping and production estimation (Bailey et al., 2001; Ribbes and Le Toan, 1999; Okamoto and Kawashima, 1999; Fang, 1998; Fang et al., 1998; Kurosu et al., 1997; Hong et al., 1997a). Inoue et al. (2000) used hyperspectral remote sensing data to measure rice canopies for estimation of plant growth. Using multitemporal Radarsat data, Shao et al. (2001) developed a method to monitor rice growth for production estimation. Shibayama et al. (1993) investigated canopy water deficit in paddy rice using a high-resolution field spectroradiometer. In another study, Shibayama and Akiyama (1989) examined rice canopy spectra with relation to leaf area index (LAI) and above ground phytomass in visible, near infrared and mid-infrared regions. Estimation of chlorophyll content in rice canopies and aboveground net production were examined in Hong et al. (1997a,b). When plants infected with pathogens, their stressed growth were morphologically displayed on the canopy due to internal damage in chlorophyll pigments and tissue structure for photosynthesis and metabolism. Consequently, the diseased plants will have different spectral features from healthy plants. Remote sensing discriminates this spectral difference to identify the diseased plants or patches in field (Zhang et al., 2003).

In spite of this potential ability, examinations of rice disease with remote sensing technology are not many up to present. One example in this aspect was

the research of Yamamoto et al. (1995), which reported remote sensing of occurrence of rice blast disease by infrared thermal image. Blast and sheath blight are the two most important rice diseases that impact rice farming in the world (Ou, 1985). The diseased plants behave differently in spectral reflectance and thermal emission from healthy ones (Zhang et al., 2003), which provide the possibility of remote sensing technology to identify the diseased plants through quantitative analysis of their spectral differences. The objectives of the study is to examine the applicability of broadband high spatial-resolution ADAR (Airborne Data Acquisition and Registration) remote sensing data in visible and near infrared to detect rice sheath blight disease, and to develop an applicable approach for practical use of the remote sensing technology. Using different combinations of the ADAR bands, we develop six band ratio indices and six band difference indices to test their correlation with disease index from field data. Then we examine the possibility of integrating the useful image indices into a remote sensing index for image process of estimating the disease severity in the field.

2. Background and study site

Rice farming in the United States is mainly concentrated in Arkansas and California, with Arkansas accounting for ~47% of US total in both acreage and production. (USDA, 1999; LaCapra et al., 1996). Experiments of the study were conducted on a large rice field in west Hazen city in central Arkansas. Sheath blight is one of the most serious rice diseases in Arkansas. An annual loss of rice yield and quality due to the blight is often greater than $80 million (USDA, 1999). Size of the field is approximately 762 m in length from north to south and 467 m in width from east to west. Geomorphologically, landscape of the region is an alluvial plain characterized with fertile black soil for agriculture. Fig. 1a shows growing conditions of rice plants in the field when samplings were conducted for evaluation of infection severity of the disease. For convenience of irrigation management, the field was divided into a number of levees (Fig. 1b).

The rice field was diagnosed with sheath blight disease, which naturally infects the rice plants in one and half month after seedlings established. Rice sheath
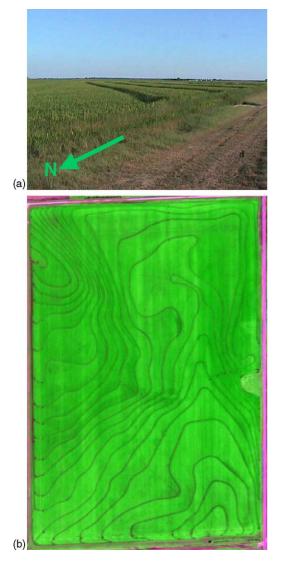
Fig. 1. (a) A ground photo of the rice field, in which levees are seen and (b) ADAR image of the rice field, acquired on July 12, 1999, with bands 3, 2, and 1 as RBG. The curved lines in the image are levees.

blight is mainly caused by fungal pathogen *Rhizoctonia solani Kühn* (Nandakumar et al., 2001; Savary et al., 1997) though some scholars such as Radja et al. (2002) and Johanson et al. (1998) believed that there was more than a single cause. Both *R. oryzae* and *R. oryzae-sativae* cause symptoms that are very similar to those of leaf blight such as sheath spot, and, lesions on leaf sheath, respectively. As a consequence, diagnosis of these diseases by ground visual observation is extremely difficult and often inaccurate, particularly at

early stages of lesion development when appropriate disease control measures must be implemented (Johanson et al., 1998).

Pathogen *Rhizoctonia solani Kühn* is both soil and water borne. Moreover, it produces a phytotoxin that could reproduce most of the symptoms of the disease (Nandakumar et al., 2001; Vidhyasekaran et al., 1997; Marshall and Rush, 1980). Currently no economically viable means are available to control the disease. Chemical means of pest management are expensive (Nandakumar et al., 2001) and have potential environmental impacts. Biological control of disease has been the focus in recent years. It is believed that the ideal bio-control agent for these pests should survive in both the rhizosphere and phyllosphere. Among various bio-control agents, strains of plant growth promoting Rhizobacteria are known to survive both in rhizosphere and phyllosphere (Krishnamurthy and Gnanamanickam, 1998).

One interesting characteristic of the disease is that primary inoculums of the disease are mainly soil-water borne, while the secondary inoculums do not consist of spores, but are predominantly in form of mycelial strands produced by primary lesions that run on the surface of leaves and sheaths to establish new lesions. As a result, epidemics usually exhibit a very strong spatial aggregation (Savary et al., 1997, 1995). Two parts are often important for observing the disease: base of rice crop canopy where primary infection predominantly occurs, and upper part of canopy where secondary infection and spread takes place (Savary et al., 1997). The terminology of 'vertical spread' and 'horizontal spread' has been used to describe sheath blight epidemics. The first refers to progress of infection along a tiller, from its base to its upper leaves by means of expanding lesions. The second refers to disease spread in crop, i.e. across tillers and rice plants (Savary et al., 1998). These characteristics are important in field samplings and image interpretation of the study.

3. Methods

3.1. Field sampling to estimate field infection severity

Field samplings were systematically conducted in the rice field during August and September 1999. The

field was divided into 11 strips, with a width of approximately 40 m for each strip except strip 11, which has a width of approximately 37 m. Field data of infection severity was estimated at each sampling site by walking centrally along each strip from east to west. The distance between two adjacent sampling sites was approximately 9 m. Thus for each strip we collected approximately 50 samples. At each site, several plants were manually examined to estimate average infection severity of the site. Three measurements were used to evaluate the severity: SHBDI = percentage of infected tillers (sheath blight) estimated by manual counting; SHBDH = height in cm of sheath blight symptoms above ground; TH = height in cm of plant canopy above soil. Finally, following the method of Nandakumar et al. (2001), we used the three field measurements to construct a comprehensive field disease index (hereafter field disease index) at laboratory for general evaluation of infection severity at each site:

$$DI_i = \frac{SHBDI_i \times SHBDH_i}{TH_i}, \tag{1}$$

where DI_i is field disease index for site i. The first sampling date (7/13/99) was ~10 days past 1/2 in. (~1.3 cm) internode elongation. The second sampling date (7/31/99) was at 100% heading. And the final rating date (8/26/99) was about a week prior to field drain for harvest.

3.2. Remote sensing image acquisition

Four airborne remote sensing images were acquired over the field on July 12, July 24, August 4, and August 17, 1999 separately during the sampling period by Positive System Inc., using ADAR (Airborne Data Acquisition and Registration) System 5500. The images had four bands respectively in blue: band 1 (450–540 nm), green: band 2 (530–600 nm), red: band 3 (610–680 nm) and near infrared: band 4 (780–1000 nm) regions. The images were stored as 8-bit digital number (DN) values ranging from 0 to 255. Ground resolution of the images was ~1 m which included approximately 150 plants. Fig. 1b shows one image of the field, with bands 3, 2 and 1 as RGB, from which one can clearly see levees of the rice field. The irregular levees were

mainly for farming irrigation management according to slope and soil variation.

3.3. Image processing to extract data

Image data were extracted to relate to the field sampling data. Using software ENVI 3.4, we generated subset images of the field from the ADAR images. Eleven strips were divided in each subset image to match strip number for field sampling. Then we calculated the row and column pixel numbers of each strip to decide the image sampling locations of the strip and computed approximate coordinate for each image sampling location. To match field sampling, we divided evenly each strip of the subset images into 50 spots for data extraction. ENVI spectral function was used for data extraction from the subset images. To minimize possible bias, we tested 4-pixel and 8-pixel schemes of data extraction for comparison. Fig. 2 shows the comparison results. Little variation was observed for the two schemes. *T*-test values for the four bands were 0.555, 0.233, 0.406 and 0.287 respectively with d.f. = 32. None of them were statistically significant at confidence level of 95%. Therefore, we concluded that there was no significant difference for these two sampling schemes. For the further analysis, 8-pixel scheme was used in the study for data extraction.

3.4. Image index computation

Three simple methods were used to capture the extracted image data for the comparison with the field
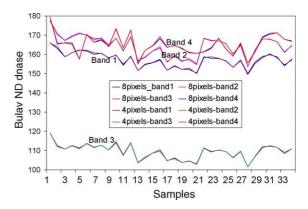

Fig. 2. Effects of different sampling schemes on sampling results for image 7/24.

disease index: (1) direct band DN value, (2) ratio indices and (3) standard difference indices. The ratio indices were calculated as follows:

$$RI_{2p} = \frac{B_2}{B_p}, \quad \text{for } p = 1, 3, 4 \tag{2a}$$

$$RI_{1q} = \frac{B_2}{B_q}, \quad \text{for } q = 3, 4 \tag{2b}$$

$$RI_{43} = \frac{B_4}{B_3}, \tag{2c}$$

where RI refers to the ratio index, B_1, B_2, B_3 and B_4 are the DN values of bands 1, 2, 3 and 4. For standard difference indices, we had:

$$SDI_{2p} = \frac{B_2 - B_p}{B_2 + B_p}, \quad \text{for } p = 1, 3, 4 \tag{3a}$$

$$SDI_{1q} = \frac{B_1 - B_q}{B_1 + B_q}, \quad \text{for } q = 3, 4 \tag{3b}$$

$$SDI_{43} = \frac{B_4 - B_3}{B_4 + B_3}, \tag{3c}$$

where SDI refers to the standard difference index. Using these indices, we expected to develop useful applicable indicators for detecting rice sheath blight in remote sensing.

3.5. Linear interpolation to match data

Since the ADAR imaging dates did not match the field sampling dates, interpolation was utilized to generate the intermediate data. Among the three field samplings and four images, only the first sampling (July 13, 1999) could be directly used to compare with the first image (July 12, 1999). Others require interpolation to match data. Linear interpolation was used in this study. Therefore for a sampling date c between two imaging dates a and b ($b > c > a$), the following formula was used:

$$DI_c = \frac{(b - c)DI_a + (c - a)DI_b}{b - a}, \tag{4}$$

where DI_c is field disease index on imaging date c, DI_a and DI_b are field disease indices on field sampling dates a and b.

Table 1
Correlation analysis of the ratio indices for sampling points with DI > 10% on image 8/4

Ratio indices	Correlation R	T test[a]
RI$_{24}$	0.67621	14.998
RI$_{23}$	0.66682	14.621
RI$_{21}$	0.26208	4.437
RI$_{14}$	0.71727	16.820
RI$_{13}$	0.60183	12.314
RI$_{43}$	0.58183	11.689

[a] All have d.f. = 267 and are statistically significant at $\alpha = 0.05$.

3.6. Method development to detect disease

Two steps were developed to process the image for disease detection. First we examined the relationships between the field disease index and the extracted image values through direct band DN values, ratio indices and standard difference indices. Then we selected useful applicable indicators to develop a method for image processing. Several indices such as RI$_{14}$, SDI$_{14}$ and SDI$_{24}$ show better correlations (Tables 1 and 2) with the field disease index. To identify infected plants from healthy ones in the field, the following procedures have been conducted for method development:

(1) Processing the images to retrieve indices RI$_{14}$, SDI$_{14}$ and SDI$_{24}$.
(2) Since the three indices have different measurement units, it is necessary to transform their values into the same magnitude system for statistical analysis. Generally two procedures are available for such transformation: "mean standard deviation" standardization method to make the values having a mean of 0 and standard deviation of 1 after transformation, and "min–max" standardization method to make the values ranging from 0

Table 2
Correlation analysis of standard difference indices for sampling points with DI > 10% on image 8/4

Image indices	Correlation R	T test[a]
SDI$_{24}$	0.60516	12.42083
SDI$_{23}$	0.58247	11.70887
SDI$_{21}$	0.26336	−4.46082
SDI$_{14}$	0.66586	14.58310
SDI$_{13}$	0.57644	11.52696
SDI$_{43}$	0.50532	−9.58636

[a] All have d.f. = 267 and are statistically significant at $\alpha = 0.05$.

to 1. In the study we select the first method for the transformation with the following formula.

$$D_{RI14} = \frac{RI_{14} - M_{RI14}}{S_{RI14}} \tag{5a}$$

$$D_{SDI14} = \frac{SDI_{14} - M_{SDI14}}{S_{SDI14}} \tag{5b}$$

$$D_{SDI24} = \frac{SDI_{24} - M_{SDI24}}{S_{SDI24}} \tag{5c}$$

where D_{RI14}, D_{SDI14} and D_{SDI24} are standardizations of RI_{14}, SDI_{14} and SDI_{24}; M_{RI14}, M_{SDI14} and M_{SDI24} are means of the indices; and S_{RI14}, S_{SDI14} and S_{SDI24} are the standard deviations.

(3) Computing a new index as an average of the three selected indices according to the following formula:

$$RSI = \frac{D_{RI14} + D_{SDI14} + D_{SDI24}}{3} \tag{6}$$

Since the three indices have a positive correlation with ground disease index, the higher value of RSI, the higher disease infection level of the pixel.

(4) Developing equation to estimate disease severity from index RSI. We divided the field sampling data into two datasets: for equation development and for validation. Data for images from July 24 and August 17 were used for equation development and image from August 4 was for validation.

(5) Validating the method. We used the RSI of image from August 4 to estimate infection severity of the sampling spots and then compared with the observed field disease index to validate the applicability of the equation. Estimated accuracy was calculated as root mean square (RMS) error in the following formula:

$$RMS = \left[\frac{\Sigma (DI' - DI)^2}{N} \right]^{1/2} \tag{7}$$

where DI' is the estimated disease index, and N number of samples for the computation. Low RMS implies high accuracy of the equation.

(6) Applying the equation to image processing. We used the equation to estimate the pixels' infection level of the image from August 4 and an estimated infection image was generated. A contour map was created using ArcView GIS from field sampling data on the imaging date to indicate infection severity of the disease. Comparisons of the estimated infection image with the contour map can demonstrate the ability of the proposed method in discriminating infected plants from healthy ones.

4. Results and discussion

4.1. Direct band DN value analysis

Fig. 3 shows direct band DN values of image August 4 of 1999 and field disease index sampled August 4 of 1999. Correlation between field disease index and direct band DN value was not apparent. The change of field disease index might be proportional to the image pixel DN values but the trend was rather weak in all bands (Fig. 3). For most pixels, the field disease index ranged from low to high and the band DN values also ranged from low to high. This widely scattering variation suggested a weak correlation between the two correspondent variables in Fig. 3, implying that the disease was difficult to be directly identified in the original wide-band images.

Correlation analysis between the field disease index and the direct band DN values indicated that only band 4 (near infrared) has relatively higher correlation ($R = 0.5928$). Using R^2, the DN values of band 4 can only explain over one third of the field disease variations. Fig. 3 also revealed that points with lower infection severity (DI < 10) did not show a clear change with the field disease index. However, the points with higher infection severity (DI ≥ 10) did show some correlated changes with the field disease index. By only using the points with DI ≥ 10, the correlation coefficients for bands 1 through 3 were much improved. When similar analysis was applied to other three images, we obtained similar results as for the image of August 4 of 1999. Thus, it was necessary to examine the applicability of image indices for the identification. Two types of image indices were examined here in the paper: band ratio indices and band difference indices.

4.2. Correlation analysis for ratio indices

Fig. 4 shows better correlations between the ratio indices and field disease index for the image of August
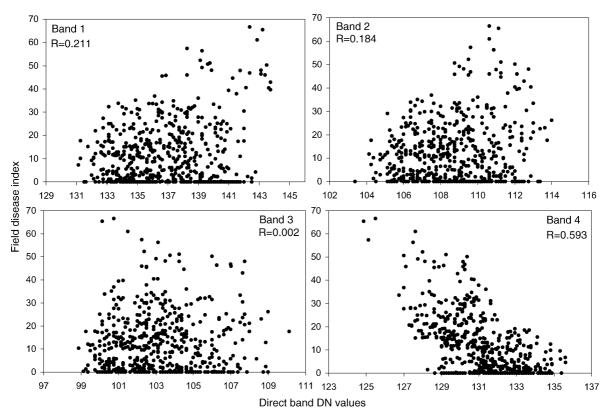
Fig. 3. Correlation between field disease index and direct band DN values for image 8/4.

4, 1999 when compared to Fig. 3. This was especially true for RI_{24}, RI_{23}, RI_{14}, and RI_{43} (Fig. 4). Fig. 4 indicates that the field disease index tends to increase with indices RI_{24}, RI_{23}, RI_{14}, and RI_{13} with statistical significance at $\alpha = 0.01$. However, for indices RI_{43} and RI_{21} the relationship was in reverse, which indicated that DI decreased with these two indices. T-test indicated that the correlation for RI_{21} was not statistically significant at $\alpha = 0.05$, which may mean that the index could not be effectively used for remote sensing of the disease. Except RI_{24}, other ratio indices had slightly better correlations, but not high enough ($R < 0.6$) to be useful either (Fig. 4). When rice plants had low infection severity (DI < 10), its spectral signature would be closer to the spectra of healthy plants. When infection severity reaches a certain level and larger spectral differences between healthy and diseased plants could be observed, discrimination of infected plants from healthy ones is possible (Zhang et al., 2002).

Figs. 3 and 4 showed that about half of the sampling points had low infection severity (DI < 10). Considering the case, we might want to see how the correlation was for only those sampling points with moderate and above infection levels. Table 1 shows the results of statistical analysis of the sampling points with DI > 10. Much better correlations were obtained in this analysis when compared to that for all sampling points. This analysis also indicated that the ratio indices RI_{24}, RI_{14}, and RI_{23} were the best three indicators (Table 1) for this disease using the remote sensing imagery.

4.3. Analysis for standard difference indices

Fig. 5 showed the correlation between field disease index and standard difference indices for image from August 4. This indicated that standard difference indices were more valuable to identify the disease than ratio indices or direct band DN values. Indices SDI_{24},
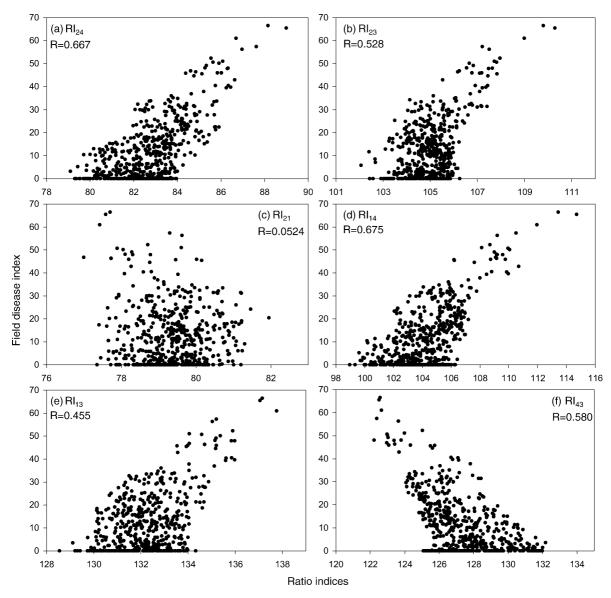
Fig. 4. Correlation between field disease index and ratio indices for image 8/4.

and SDI$_{14}$ were better than indices SDI$_{23}$, SDI$_{23}$ and SDI$_{43}$ (Fig. 5). The first two indices explained 40% of the variation of field disease index, while the latter three only explained 17–23%. The index SDI$_{21}$, most scattering, had almost no correlation with the field disease index.

Using only the points with DI ≥ 10, the correlation coefficients were higher than those for all sampling points (Table 2). This confirmed the previous

conclusion that detection of the rice disease was possible only when infection severity reaches a certain level. Even though there were differences among the images of early and late growing seasons, some image indices especially SDI$_{24}$, SDI$_{14}$, SDI$_{23}$, SDI$_{43}$ and SDI$_{13}$ were better correlated (Table 2) with the field disease index in all cases. These indices could be valuable indicators for developing method to detect the rice disease in remote sensing.
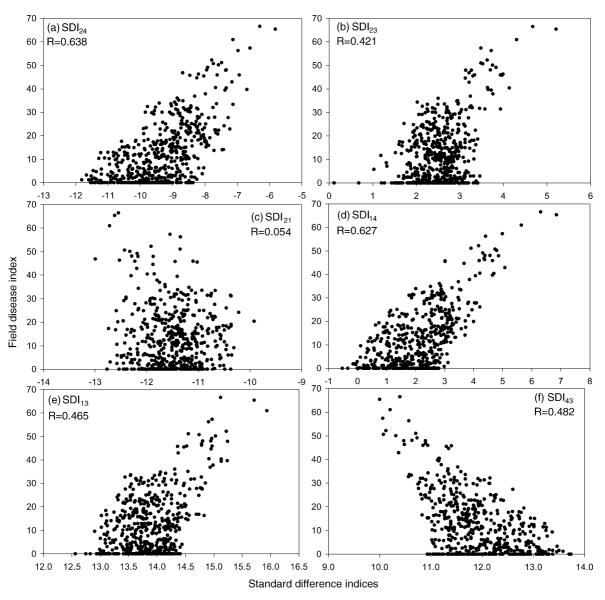
Fig. 5. Correlation between field disease index and standard difference index for image 8/4.

4.4. Statistical analysis for indicator selection

The above analysis revealed that standard difference indices were better correlated with the field disease index than any of the single band and ratio indices. Furthermore, Tables 1 and 2 indicated that indices RI_{24}, RI_{14}, RI_{23}, SDI_{24}, SDI_{14}, and SDI_{43} had relatively higher correlation with the field disease index for image from August 4. Table 3 showed that

indices RI_{14}, SDI_{24} and SDI_{14} were generally better than other indices. Their correlations coefficients were 0.675, 0.638 and 0.627 respectively for image 8/4, and 0.622, 0.708 and 0.564 for image 8/17. These values were statistically significant at confidential level above 99%. The higher correlations of these three indices were observed in later images (8/4 and 8/17) than in early image (7/24). This might attribute to the different development stages of the rice disease in the

Table 3
Correlation analysis of the highlighted indices for all images

Image indices	Correlation R	T test[a]
Image 7/24		
RI_{24}	0.41570	10.69950
RI_{14}	0.30810	7.58123
RI_{43}	0.31786	10.7465
SDI_{24}	0.41642	10.72188
SDI_{14}	0.45025	11.80429
SDI_{43}	0.30757	7.56695
Image 8/4		
RI_{24}	0.66704	20.95891
RI_{14}	0.67458	21.39170
RI_{43}	0.57993	16.66408
SDI_{24}	0.63819	19.40523
SDI_{14}	0.62664	18.82342
SDI_{43}	0.48223	12.89783
Image 8/17		
RI_{24}	0.45891	12.09119
RI_{14}	0.62170	18.58107
RI_{43}	0.47662	12.69154
SDI_{24}	0.70784	23.45816
SDI_{14}	0.56438	16.00450
SDI_{43}	0.42694	11.05220

[a] All have d.f. = 548 and are statistically significant at $\alpha = 0.05$.

field, in spite of the fact that different treatments of pesticides have been applied for other projects. In later images, the disease may have progressed in severity than in early days. This in turn affects the spectral signature of the plants for remote sensing. Since these indices have generally higher correlation with the field disease index, we may conclude that they are better candidate indicators for remote sensing identification of the rice disease.

4.5. Classification analysis of rice disease severity

Using Eq. (6), we developed a comprehensive image index on the basis of the selected indices RI_{14}, SDI_{24} and SDI_{14} to classify the images. We classified the images into four classes, with class 1 referring to healthy to light infection (DI < 20), class 2 referring to light to moderate infection (DI = 20–35), class 3 referring to moderate to severe infection (DI = 35–50), and class 4 referring to severe infection (DI > 50). Fig. 6 indicated that the points with RSI < 2 mainly corresponded to the samples of DI < 20, RSI ranging from 0 to 1.5 mainly to the samples of DI between 20
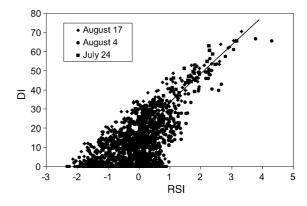

Fig. 6. Correlations between RSI and DI for remote sensing of the rice disease. The lines inside is the fitted regression equation.

and 25, RSI ranging from 1.5 to mainly to the samples of DI between 35 and 50, and RSI > 2.5 mainly to those samples with DI > 50. Therefore, we used the following criteria: RSI < 0.5 for class 1, RSI = 0.5–1.5 for class 2, RSI = 1.5–2.5 for class 3 and RSI > 2.5 for class 4 for the classification of the images. The accuracy of the classification was ∼76% (Table 4). The misclassification was mainly from in class 2 of some light infection samples, which in practice might benefit pest management in fields to control the disease at early stage.

4.6. Equation for estimation of infection severity

Using the comprehensive image indices for the dataset of images 7/24 and 8/17, we were able to develop an equation for quantitative estimation of the infection level of rice plants in the remote sensing imagery:

$$DI = 12.74001 + 10.42501\,RSI$$
$$R = 0.606 \qquad SEE = 10.848 \qquad F = 637.2 \qquad (8)$$

The relationship between the field disease index and the RSI was statistically significant. The standard estimation error (SEE) implied that the disease index estimate was probably with an average error of 10.8 using the equation. Considered moderate infection when DI was over 35, this estimation error might still be acceptable to take management actions in the field. The correlation of the equation was only 0.606, which was somewhat low. This relatively low correlation

Table 4
Accuracy of classification with the image index

Image	Class	Correct	Mis-class	Accuracy (%)
7/24	1	396	18	83.54
	2	22	35	38.60
	3	12	6	66.67
	4	1	0	100.00
	Sum	431	119	78.36
8/4	1	361	39	90.25
	2	60	64	48.39
	3	12	9	57.14
	4	4	1	80.00
	Sum	437	113	79.45
8/17	1	335	61	84.60
	2	48	81	37.21
	3	10	6	62.50
	4	9	0	100.00
	Sum	402	148	73.09
Total	1	1092	178	85.98
	2	130	180	41.94
	3	34	21	61.82
	4	14	1	93.33
	Sum	1270	380	76.97

may imply the limitation of the wide-band imaging data in disease detection. It is applicable for disease detection but not as good as we expect!

We validated the equation to another ground sampling dataset (image 8/4), which resulted in a root mean square (RMS) error of 9.555. The smaller of RMS than SEE confirmed the higher accuracy of the equation for estimation. However, Eq. (8) may result in DI < 0, which contradicted our assumption of healthy plants having DI = 0. Moreover, we found that the estimation could be improved for the points with DI > 10:

$$DI = 13.61421 + 15.195263\,RSI$$
$$R = 0.683 \quad SEE = 9.322 \qquad F = 682.6 \qquad (9)$$

Actually RSI = −1.115 and −0.240, respectively corresponded to DI = 0 and 10 when Eq. (8) was used. Therefore, the following strategy was proposed for estimation of infection severity in practical application: (a) let DI = 0 when RSI < −1.115, (b) use Eq. (8) when −1.115 < RSI < −0.240, and (c) use Eq. (9) when RSI > −0.240. Applying this strategy to image 8/4 resulted in Fig. 7, which showed the estimated DI against the observed DI. This strategy produced a
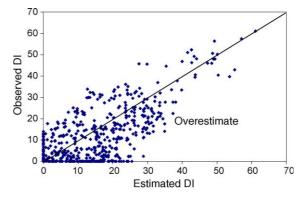

Fig. 7. Comparison of the estimated DI with the observed DI on image 8/4 for validation. The diagonal represents no error.

smaller estimation of RMS = 9.104 to image 8/4 than Eq. (8). Fig. 7 showed overestimates for DI values between 15 and 35, which corresponded to light-to-moderate infection level. Such an overestimate might be favorable for pest management because it provided higher alert to disease controls before severe development of the disease.

4.7. Distribution of the rice disease on images

Fig. 8a displays the disease severity in the field after image classifications and Fig. 8b presents the disease severity from field samplings. Both field maps had similar patterns of disease severity. Comparisons of the GIS contour mapping of field scouting points for the disease infection levels (Fig. 8b) with the image disease classifications (Fig. 8a) indicate that the method of predicting the disease severity from imagery was applicable for the disease identification. The estimated infected areas in the image overlapped the spatial patterns of the observed disease identified in the GIS contour map. Geostatistical analysis of the image and the counter map results in a spatial correlation of 0.668 between the image and the map for the sampling locations identified partly on the map (Fig. 8b). This correlation is slightly lower than the correlation of Eq. (9) used to generate the image. This may be attributed to the date difference of the image (8/4) and the map (7/31). The analysis also indicates that the RMS error of the image to the map is 11.56, also higher than the SEE error of Eq. (9), probably as a result of its lower correlation than the equation's correlation. By scaling into the classes, we find that the

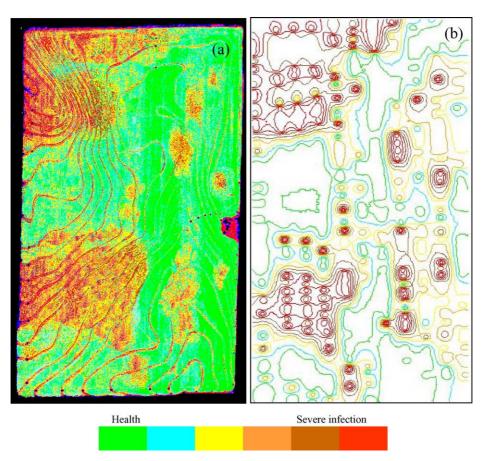Health   Severe infection

Fig. 8. Spatial patterns of sheath blight infection in the rice field. (a) Retrieved infection from image 8/4 using our method and (b) contour of the disease severity based on field sampling data obtained on July 31, 1999.

image has 68.63% of the sampling locations sharing the same infection severity as the map, indicating that accuracy of the estimation by the approach is slightly higher than 2/3.

In spite of this, the image illustrated the detailed spatial distribution of the disease and showed the possible disease development in the field. Two main infected areas were clearly identified in the image. The upper left part and the middle-to-lower part in the image corresponded to the two main infected areas. In general, the western half of the rice field was much more severely infected with sheath blight than its eastern half. On the other hand, we also noticed that the plants along the levees had higher level of infection. This might imply an infection pattern of the disease development along levees. Levees served as irrigation and venture channel for the field. These might provide better

conditions for the disease (fungus spores) to propagate spatially in the field because water was a favorable factor for the development of pathogen *Rhizoctonia solani Kühn* leading to sheath blight (Nandakumar et al., 2001; Vidhyasekaran et al., 1997).

Although the distribution of the image extracted infection generally matched with the GIS contour mapping of the infection, there were differences of infections severity between Fig. 8a and b. The GIS contour map showed more extensively the moderate infection than that on the ADAR image. This was likely attributed to the accuracy of the method, which was ~70% as mentioned above. On the other hand, ADAR was a broadband imagery system. In spite of high spatial resolution (1 m), its spectral resolution was quite low. The four bands cover broader range of blue, green, red and infrared wavelengths. Since infected plants do

not show an obvious spectral difference from healthy ones in broad range of visible wavelength (Zhang et al., 2002), the broadband ADAR images might not be able to accurately separate infection severity in these wavelengths. This implied that the ADAR system was highly valuable in remote sensing of crop disease detection but its spectral resolution might not be high enough to accurately discriminate plants with light infections. In Japan, Yamamoto et al. (1995) examined the applicability of infrared thermal images in identification of rice blast disease through visual interpretation. Though the occurrence of rice blast disease was visible in thermal images, quantitative analysis using various indices for accurate identification had not been done in their study. Our study showed that ADAR images could be used to show the coarse distribution patterns of infected plants in the field. To accurately map the severity of infected plants, a better spectral resolution imagery system is required (narrower bandwidth and more bands especially in infrared range), in addition to high spatial resolution. Hyperspectral remote sensing and thermal remote sensing may be such alternatives (Zhang et al., 2003).

5. Conclusion

This research using the broadband visible and infrared data in the study indicates that remote sensing technology could offer great potential in application to detect crop disease. Actual application of the technology in field pest management would come later. Direct band DN values did not show an encouraging correlation with field-sampled disease severity. Band ratio indices and standard difference indices had the potential to serve as indicators for remote identification of rice sheath blight. Among the six band ratio indices and six standard difference indices, we found that RI_{14}, SDI_{14} and SDI_{24} were generally better in correlating with field disease index to indicate the infection levels of the rice disease. The significant correlations between these three indices and the field disease index confirmed the capability of broadband airborne multispectral remote sensing imagery in identifying the rice disease.

On the basis of these three indices, a method had been developed in the study, including to retrieve the three indices from original image data and to convert them into the same scaling through standardization. For practical use, a method had been developed to combine these three indices into a comprehensive image index (RSI) for classifying the rice disease. Finally, we applied the comprehensive index to classify four classes. Validation with the ground data indicated that this scheme had an accuracy of up to 70%.

A strategy with two corresponding equations had been developed for quantitative estimation of the disease severity using the comprehensive image index. As indicated by F test value, the equations were statistically significant, indicating that they were applicable. Similar spatial distribution of image detected disease patterns and the ground scouting patterns in the field confirmed the applicability of the proposed method. Spatial accuracy of the method was 68.63% for the sampling locations when the estimation from 8/4 image was compared with the 7/31 counter map (Fig. 8). We also realized from our analysis that discrimination of healthy plants from light infection ones (DI < 20) was difficult because of their heavy overlap in the estimated image indices. Identification was more accurate when infection reached to moderate to severe level (DI > 35). This might suggest that, in addition to high spatial resolution, a better spectral resolution remote sensing imagery with more bands and narrower bandwidth would be highly required for remote sensing diagnosis of crop disease stress.

Acknowledgements

References

Bailey, K.D., Frohn, R.C., Beck, R.A., Price, M.W., 2001. Remote sensing analysis of wild rice production using Landsat 7 for the Leech Lake band of Chippewa in Minnesota. Photogram. Eng. Rem. Sens. 67 (2), 189–192.

Cline, B.L., 1970. New eyes for epidemiologists, aerial photography and other remote sensing techniques. Am. J. Epidemiol. 92, 85–89.

Fang, H., 1998. Rice crop area estimation of an administrative division in China using remote sensing data. Int. J. Rem. Sens. 19 (17), 3411–3419.

Fang, H., Wu, B., Liu, H., Huang, X., 1998. Using NOAA AVHRR and Landsat TM to estimate rice area year-by-year. Int. J. Rem. Sens. 19 (3), 521–525.

Hay, S.I., 1997. Remote sensing and disease control: past, present and future. Trans. R. Soc. Trop. Med. Hygiene 91, 105–106.

Hong, S., Lee, J., Rim, S., Shin, J., 1997a. Radiometric estimates of grain yields related to crop aboveground net production (ANP) in paddy rice. In: Proceedings of the International Geoscience and Remote Sensing Symposium, 4. pp. 1793–1795.

Hong, S., Rim, S., Lee, J., Kim, J., 1997b. Remote sensing for estimating chlorophyll amount in rice canopies. In: Proceedings of the International Geoscience and Remote Sensing Symposium, 1. pp. 89–91.

Inoue, Y., Qi, J., Nouvellon, Y., Moran, M.S., 2000. Hyperspectral and directional remote sensing measurements of rice canopies for estimation of plant growth variables. In: Proceedings of the International Geoscience and Remote Sensing Symposium, 4. pp. 1471–1473.

Johanson, A., Turner, H.C., McKay, G.J., Brown, A.E., 1998. A PCR-based method to distinguish fungi of the rice sheath-blight complex, *Rhizoctonia solani*, *R. oryzae* and *R. oryzae-sativae*. FEMS Microbiol, Lett. 162, 289–294.

Krishnamurthy, K., Gnanamanickam, S.S., 1998. Biological control of rice blast by Pseudomonas fluorescens strains Pf7-14: evaluation of a marker gene and formulations. Biol. Contr. 13, 158–165.

Kurosu, T., Fujita, M., Chiba, K., 1997. Identification of rice fields using multi-temporal ERS-1 C band SAR data. Int. J. Rem. Sens. 18 (14), 2953–2965.

LaCapra, V.C., Melack, J.M., Gastil, M., Valeriano, D., 1996. Remote sensing of foliar chemistry of inundated rice with imaging spectrometry. Rem. Sens Environ. 55 (1), 50–58.

Marshall, D.S., Rush, M.C., 1980. Infection cushion formation on rice sheaths by *Rhizoctonia solani*. Phytopathology 70, 947–950.

Nandakumar, R., Babu, S., Viswanathan, R., Raguchander, T., Samiyappan, R., 2001. Induction of systemic resistance in rice against sheath blight disease by *Pseudomonas fluorescens*. Soil Biol. Biochem. 33, 603–612.

Okamoto, K., Kawashima, H., 1999. Estimation of rice-planted area in the tropical zone using a combination of optical and microwave satellite sensor data. Int. J. Rem. Sens. 20 (5), 1045–1048.

Ou, S.H., 1985. Rice diseases, 2nd ed. Common wealth Mycological Institute, Kew, Survey, England, 380 pp.

Radja C.R., Nandakumar, R., Kandan, A., Suresh, S., Bharathi, M., Raguchander,T., Samiyappan, R., 2002. *Pseudomonas fluorescens* based bio-formulation for the management of sheath blight disease and leaf-folder insect in rice. Crop Protect. 21 (8), 671–677.

Ribbes, F., Le Toan, T., 1999. Rice field mapping and monitoring with RADARSAT data. Int. J. Rem. Sens. 20 (4), 745–765.

Savary, S., Castilla, N.P., Elazegui, F.A., McLaren, C.G., Ynalvez, M.A., Teng, P.S., 1995. Direct and indirect effects of nitrogen supply and disease source structure on rice sheath blight spread. Phytopathology 85, 959–965.

Savary, S., Elazegui, F.A., Teng, P.S., 1998. Assessing the representativeness of data on yield losses due to rice diseases in tropical Asia. Plant Dis. 82 (6), 705–709.

Savary, S., Willocquet, L., Teng, P.S., 1997. Modelling sheath blight epidemics on rice tillers. Agric. Syst. 55 (3), 359–384.

Shao, S., Fan, H., Liu, J., Xiao, S., Ross, B., Brisco, R., Brown, Staples, G., 2001. Rice monitoring and production estimation using multitemporal RADARSAT. Rem. Sens. Environ. 76 (3), 310–325.

Shibayama, M., Takahashi, W., Morinaga, S., Akiyama, T., 1993. Canopy water deficit detection in paddy rice using a high resolution field spectroradiometer. Rem. Sens. Environ. 45 (2), 117–126.

Shibayama, M., Akiyama, T., 1989. Seasonal visible, near-infrared and mid-infrared spectra of rice canopies in relation to LAI and above-ground dry phytomass. Rem. Sens. Environ. 27 (2), 119–127.

United States Department of Agriculture (USDA), 1999. Agricultural Statistics, Washington, DC.

Vidhyasekaran, P., Ponmalar, T., Samiyappan, R., Velazhahan, R., Vimala, R., Ramanathan, A., Paranitharan, V., Muthukrishnan, S., 1997. Host specific toxin production by *Rhizoctonia solani*, the rice sheath blight pathogen. Phytopathology 87, 1258–1263.

Yamamoto, H., Suzuki, Y., Iwano, M., Hayakawa, S., 1995. Remote sensing of occurrence place of rice blast disease by infrared thermal image. Jpn. J. Crop Sci. 64 (3), 467–474.

Zhang, M., Liu, X., O'Neill, M., 2002. Spectral discrimination of phytophthora infestans infection on tomatoes based on principle component and cluster analyses. Int. J. Rem. Sens. 23 (6), 1095–1107.

Zhang, M., Qin, Z., Liu, X., Ustin, S.L., 2003. Detection of stress in tomatoes induced by late blight disease in California, USA, using hyperspectral remote sensing. Int. J. Appl. Earth Observ. Geoinf. 4, 295–310.